Spatial inter-centromeric interactions facilitated the emergence of evolutionary new centromeres

Krishnendu Guin[1], Yao Chen[2], Radha Mishra[1], Siti Rawaidah B. M. Muzaki[2], Bhagya C. Thimmappa[1], Caoimhe E. O'Brien[3], Geraldine Butler[3], Amartya Sanyal[2*], Kaustuv Sanyal[1, 4*]

[1]Molecular Mycology Laboratory, Molecular Biology and Genetics Unit, Jawaharlal Nehru Centre for Advanced Scientific Research, Bangalore 560064, India; [2]School of Biological Sciences, Nanyang Technological University, 60 Nanyang Drive, Singapore 637551; [3]School of Biomolecular & Biomed Science, Conway Institute of Biomolecular and Biomedical Research, University College Dublin, Belfield, Dublin 4, Ireland. [4]Graduate School of Frontier Biosciences, Osaka University, Suita, Osaka 565 0871, Japan

*corresponding author

Kaustuv Sanyal, Ph.D.
Molecular Biology & Genetics Unit
Jawaharlal Nehru Centre for Advanced Scientific Research
Jakkur, Bangalore – 560064
India
Email: sanyal@jncasr.ac.in
Telephone : +91 80 2208 2878
Fax : +91 80 2208 2766

Amartya Sanyal, Ph.D.
School of Biological Sciences
Nanyang Technological University
60 Nanyang Drive, SBS-05n-22
Singapore 637551
Email: asanyal@ntu.edu.sg
Telephone: (+65) 6513-8270

Present address:
Bhagya C. Thimmappa, Department of Biochemistry, Robert-Cedergren Centre of Bioinformatics and Genomics, University of Montreal, Montreal, QC H3T 1J4, Canada.
Radha Mishra, Department of Cellular & Molecular Medicine, University of Ottawa, ON K1H 8M5, Canada.

Classification:
Biological Science, Genetics

Keywords:
Genome assembly, 3D genome, 3C-seq, CUG-Ser1 clade, Evolutionary new centromere, Chromosome segregation

Abstract

Centromeres of *Candida albicans* form on unique and different DNA sequences but a closely related species, *Candida tropicalis*, possesses homogenized inverted repeat (HIR)-associated centromeres. To investigate the mechanism of centromere-type transition, we improved the fragmented genome assembly and constructed a chromosome-level genome assembly of *C. tropicalis* by employing PacBio sequencing, chromosome conformation capture sequencing (3C-seq), chromoblot, and genetic analysis of engineered aneuploid strains. Further, we analyzed the 3D genome organization using 3C-seq data, which revealed spatial proximity among the centromeres as well as telomeres of seven chromosomes in *C. tropicalis*. Intriguingly, we observed evidence of inter-centromeric translocations in the common ancestor of *C. albicans* and *C. tropicalis*. Identification of putative centromeres in closely related *Candida sojae*, *Candida viswanathii* and *Candida parapsilosis* indicates loss of ancestral HIR-associated centromeres and establishment of evolutionary new centromeres (ENCs) in *C. albicans*. We propose that spatial proximity of the homologous centromere DNA sequences facilitated karyotype rearrangements and centromere type transitions in human pathogenic yeasts of the CUG-Ser1 clade.

Introduction

The efficient maintenance of the genetic material and its propagation to subsequent generations determine the fitness of an organism. Genomic rearrangements are often associated with the development of multiple diseases, including cancer. Chromosomal rearrangements, on the other hand, are often observed during speciation (1). Such structural changes begin with the formation of at least one DNA double-strand break (DSB), which is generally repaired by homologous recombination (HR) or non-homologous end joining (NHEJ) *in vivo*. Studies using engineered *in vivo* model systems suggested that the success of DSB repair through HR depends upon an efficient identification of a template donor. This process of ‘homology search’ is facilitated by the physical proximity and the extent of DNA sequence homology (2-4). Multi-invasion-induced rearrangements (MIRs) involving more than one template donors have recently been shown to be influenced

85 by physical proximity and homology (5). Therefore, the nature of genomic
86 rearrangements is mostly dependent on the type of spatial genome organization. In
87 yeasts, apicomplexans, and certain plants, centromeres cluster inside the nucleus
88 (6), which may facilitate translocations between two chromosomes involving their
89 centromeric and adjacent pericentromeric loci.
90
91 The centromere, one of the guardians of genome stability, assembles a large
92 DNA-protein complex to form the kinetochore, which ensures fidelity of chromosome
93 segregation by correctly attaching chromosomes to the spindle. Paradoxically, this
94 conserved process of chromosome segregation is carried out by highly diverse
95 species-specific centromere DNA sequences. For example, the length of centromere
96 DNA is ~125 bp in budding yeast *Saccharomyces cerevisiae* (7), but it can be as
97 long as a few megabases in humans (8). Centromeres have been cloned and
98 characterized from a large number of fungal species. The only factor that remains
99 common to most fungal centromeres is the presence of histone H3 variant CENP-
100 A^{Cse4} except in some Mucorales like *Mucor circinelloides* (9). Many kinetochore
101 proteins are believed to have evolved from pre-eukaryotic lineages and remained
102 conserved within closely related species complexes or expanded through gene
103 duplication (10-12). It remains a paradox that despite the rapid evolution of
104 centromere DNA, the kinetochore structure remains relatively well-conserved (13).
105 Therefore, an examination of the evolutionary processes driving species-specific
106 changes in centromere DNA is essential for a better understanding of centromere
107 biology.
108
109 The first cloned centromere that of the budding yeast *S. cerevisiae* carries
110 conserved genetic elements capable of forming a functional centromere *de novo*
111 when cloned into a yeast replicative plasmid (7). Such genetic regulation of
112 centromere function also exists in the fission yeast *Schizosaccharomyces pombe,*
113 where centromeres possess inverted repeat-associated structures of 40-100 kb (14).
114 Other closely related budding and fission yeasts were also found to harbor a DNA
115 sequence-dependent regulation of centromere function (15-17), but the advantage of
116 having such genetic regulation is not well understood. In fact, the majority of species
117 with known centromeres are thought to be regulated by an epigenetic mechanism
118 (13). A truly epigenetically-regulated fungal centromere carrying a 3-5 kb long

119 CENP-A^{Cse4}-bound unique DNA sequence exists in another budding yeast *C.*
120 *albicans* (18), a CUG-Ser1 clade species in the fungal phylum of Ascomycota.
121 Subsequently, such unique centromeres were also discovered in closely related
122 *Candida dubliniensis* (19) and *Candida lusitaniae* (20). Strikingly, all seven
123 centromeres of *C. tropicalis,* another CUG-Ser1 clade species, carry 3-4 kb long
124 inverted repeats (IR) flanking ~3 kb long CENP-A^{Cse4} rich central core (CC). The
125 centromere sequences are highly identical to each other in *C. tropicalis*. Intriguingly,
126 centromere DNA of *C. tropicalis* can facilitate *de novo* recruitment of CENP-A^{Cse4} to
127 some extent (21). In contrast, centromeres of *C. albicans* completely lack such a
128 DNA sequence-dependent mechanism (22). Such a rapid transition in the structural
129 and functional properties of centromeres within two closely related species offers a
130 unique opportunity to study the process of centromere type transition.
131
132 Kinetochore proteins appeared as a single punctum at the periphery of a
133 nucleus indicating the presence of constitutively clustered centromeres in *C.*
134 *tropicalis* (21). Our previous analysis also showed that centromeres of *C. tropicalis*
135 were located near interchromosomal synteny breakpoints (ICSBs) as relics of
136 ancient translocations in the common ancestor of *C. tropicalis* and *C. albicans* (21).
137 Do homologous centromere DNA regions in close spatial proximity facilitate
138 chromosomal translocation events? Due to the nature of the then-available
139 fragmented genome assembly, the genome-wide distribution of the ICSBs and the
140 spatial organization of the genome in *C. tropicalis* remained unexplored. However,
141 the near-complete *C. albicans* genome assembly was available. Therefore, to
142 examine whether the spatial proximity of clustered centromeres drives
143 interchromosomal translocation events guiding speciation in the CUG-Ser1 clade
144 required a chromosome-level complete genome assembly of *C. tropicalis*.
145
146 In this study, we constructed a chromosome-level gapless genome assembly
147 of the *C. tropicalis* type strain MYA-3404 by combining information from previously
148 available contigs, NGS reads and high-throughput 3C-seq data. Using this assembly
149 and 3C-seq data, we studied the spatial genome organization in *C. tropicalis.* Next,
150 we mapped the ICSBs in the *C. tropicalis* genome with reference to that of *C.*
151 *albicans* (ASM18296v3) to test whether the frequency of ICSB correlated with the
152 spatial genome organization. In addition, we performed Oxford Nanopore and

153 Illumina sequencing and assembled the genome of *Candida sojae* (strain NCYC-
154 2607), a sister species of *C. tropicalis* in the CUG-Ser1 clade (23). Finally, using this
155 genome assembly of *C. sojae* and publicly available genome assembly of *C.*
156 *viswanathii* (ASM332773v1), we identified the putative centromeres of these two
157 species as HIR-associated loci syntenic to the centromeres of *C. tropicalis*. Based on
158 our results, we propose a model that suggests homology and proximity guided
159 centromere-proximal translocations facilitated karyotype evolution and possibly aided
160 in rapid transition from HIR-associated to unique centromere types in the members
161 of the CUG-Ser1 clade.
162

163 **Results**

164 **A chromosome-level gapless assembly of the *C. tropicalis* genome in seven**
165 **chromosomes**

166 *C. tropicalis* has seven pairs of chromosomes (21, 24). However, the current
167 publicly available genome assembly (ASM633v3) has 23 nuclear contigs and one
168 mitochondrial contig. To completely assemble the nuclear genome of *C. tropicalis* in
169 seven chromosomes, we combined results of short-read Illumina sequencing and
170 long-read single molecule real-time sequencing (SMRT-seq) with high-throughput
171 3C-seq (simplified Hi-C) experiment (Figure 1A, S1A-D) (25). We started from the
172 publicly available genome assembly of *C. tropicalis* strain MYA-3404 in 23 nuclear
173 contigs (ASM633v3, Assembly A) (24). We used Illumina sequencing reads to
174 scaffold them into 16 contigs to get Assembly B (Figure 1A). Next, we used the
175 SMRT-seq long reads to join these contigs, which resulted in an assembly of 12
176 contigs (Assembly C, Table S1). Based on the contour clamped homogenized
177 electric field (CHEF)-gel karyotyping (Figure 1B) and 3C-seq data (Figure S1E-G),
178 we joined two contigs and rectified a misjoin in Assembly C to produce an assembly
179 of seven chromosomes and five short orphan haplotigs (OHs). We suspected that
180 the OHs are heterozygous loci in the diploid genome of *C. tropicalis*. Analysis of the
181 *de novo* contigs (Figure S1H, Methods), sequence coverage data (Figure S2A-B),
182 and Southern hybridization of engineered aneuploid strains demonstrated that the
183 small OHs mapped to heterozygous regions of the genome (Figure S2C-I, Methods).
184 Next, we used *de novo* contigs to fill pre-existing 104 N-gaps and scaffolded 14 sub-
185 telomeres (Figure S3A-C, Table S2). Finally, we used 3C-seq reads to polish the
186 complete genome assembly of *C. tropicalis* constituting 14,609,527 bp in seven

187 telomere-to-telomere long gapless chromosomes (Figure 1B). We call this new
188 assembly as Assembly2020.
189
190 We assigned the numbers to each chromosome according to the length,
191 starting from the longest as chromosome 1 (Chr1) through the shortest as
192 chromosome 6 (Chr6). The remaining chromosome, the one containing the rDNA
193 locus, was named as chromosome R (ChrR) (Figure 1C). Accordingly, centromeres
194 on each chromosome were named after the respective chromosome number.
195 Additionally, we oriented the DNA sequence of each chromosome in a way to
196 consistently maintain the short arm at the 5′ end. The statistics of these genome
197 assemblies of *C. tropicalis* is summarized in Table S3. In Assembly2020, 1278 out of
198 1315 Ascomycota-specific BUSCO gene sets could be identified compared to 1255
199 identified using Assembly A (Table S4, Methods). The inclusion of 23 additional
200 BUSCO gene sets suggests significantly improved contiguity and completeness of
201 Assembly2020.
202
203 Previously, using centromere-proximal probes, we could distinctly identify five
204 chromosomes (Chr1, Chr2, Chr3, Chr5, and Chr6) in chromoblot analysis (21).
205 However, the lengths of Chr4 and ChrR could not be determined. To validate the
206 correct assembly of these two chromosomes (Chr4 and ChrR), we performed
207 additional chromoblot analysis. We observed that Chr4 homologs differed in size
208 (Figure S4A). Analysis of the sequence coverage across Chr4 identified a substantial
209 internal duplication of ~235 kb region, which could explain the size difference
210 between the homologs Chr4A and Chr4B (Figure 1C, S4B). We named this
211 duplicated locus as *DUP4.* Subsequently, we scanned the entire genome for the
212 presence of copy number variations (CNVs), which led to the identification of two
213 additional large-scale duplication events: one each on Chr5 (*DUP5*, ~23 kb) and
214 ChrR (*DUPR*, ~80 kb) (Figure 1C, S4B). Further, using CNAtra software (26) we
215 confirmed these duplication events and identified additional small-scale CNV loci
216 with copy number <1.5 or >2.5 (Figure S4C). Additionally, we detected a balanced
217 heterozygous translocation event between Chr1 and Chr4 (Figure S5A) through
218 analyses of 3C-seq data and *de novo* contigs (Figure S5B). This translocation was
219 validated using chromoblot analysis (Figure S5C) as well as Illumina, and SMRT-seq

220 read mapping (Figure S5D). Thus, while chromoblot analysis suggests that the
221 actual length of ChrR is ~2.8 Mb (Figure S5E), the assembled length is 2.1 Mb
222 (Figure 1C). Considering the length of the rDNA locus is ~700 kb in *C. albicans* (27),
223 we reason that the difference between the assembled length and actual length
224 (derived from chromoblot analysis) of ChrR in *C. tropicalis* can be attributed to the
225 presence of the repetitive rDNA locus of ~700 kb, which is not completely assembled
226 in Assembly2020.
227
228 Next, we performed phasing of the diploid genome of *C. tropicalis* using
229 SMRT-seq and 3C-seq data to identify the homolog-specific variations (Methods).
230 This analysis produced 16 nuclear contigs, which were colinear with the
231 chromosomes of Assembly2020, except for the previously validated heterozygous
232 translocation between Chr1 and Chr4 (Figure S5F). To characterize the sequence
233 variations in the diploid genome of *C. tropicalis,* we identified the single nucleotide
234 polymorphisms (SNPs) and insertion-deletion (indel) mutations (Methods).
235 Intriguingly, we detected a long chromosomal region depleted of SNPs and indels on
236 the left arm of ChrR (Figure 1D). We named this region that lost heterozygosity on
237 ChrR as LOH^R. Strikingly, we found parts of the syntenic region of LOH^R to be SNP
238 and indel depleted in the *C. sojae* strain NCYC-2607, a closely related species of *C.*
239 *tropicalis*, as well as in *C. albicans* reference strain SC5314 (Figure S6). We also
240 identified the genome-wide distribution of transposons and simple repeats but could
241 not detect preferential enrichment of these sequence elements at any specific
242 genomic location in *C. tropicalis* (Figure 1D). Together, we demonstrate, for the first
243 time, multiple CNVs, a long-track LOH, and evidence of a heterozygous reciprocal
244 translocation event in the diploid genome of *C. tropicalis.* Possible implications of
245 these events in conferring virulence and drug resistance in this successful human
246 fungal pathogen remain to be explored.
247
248 **Conserved principle of the spatial genome organization in *C. tropicalis* and *C.***
249 ***albicans***
250 Indirect immunofluorescence imaging of the *C. tropicalis* strain (CtKS102)
251 expressing Protein-A tagged CENP-A^{Cse4} suggested that centromeres are clustered
252 and localized at the periphery of the DAPI-stained nuclear DNA mass as a single
253 punctum (Figure 2A-B). We mapped 3C-seq data (see Methods), that were

generated using DpnII, to the Assembly2020 to construct the genome-wide chromatin contact map of *C. tropicalis*. The resultant heatmap depicts high signal intensities along the diagonal, indicating that the intrachromosomal interactions are generally stronger than interchromosomal interactions, as observed before (Figure 2C) (28). However, the most striking feature of the heatmap is the presence of conspicuous puncta in the interchromosomal areas, which signify strong spatial proximity between centromeres (Figure 2C-D). The aggregate signal analysis further reiterated the enrichment of centromere-centromere interactions (Figure 2E). Strikingly, we also noted the enrichment of telomere-telomere interactions as compared to the neighboring regions (Figure 2C-E). Statistical comparison was then performed between these telomere-telomere interactions and bulk chromatin, which revealed that the interchromosomal telomeric interactions were significantly greater than the all interchromosomal interactions (Mann-Whitney U test P value = $1.129 \cdot 10^{-11}$) (Figure S7A). On the other hand, *cis* interactions between the two telomeres of an individual chromosome (intrachromosomal telomeric interactions) were also significantly enhanced compared to all intrachromosomal long-range (>100 kb) interactions (Mann-Whitney U test P value = $7.374 \cdot 10^{-11}$) (Figure S7B). All these lines of evidence prompted us to propose that *C. tropicalis* chromosomes adopt the Rabl-like configuration, a characteristic feature of the higher-order genome organization in yeasts (28-30).

Previously, microscopic and Hi-C studies revealed similar centromere clustering and strong physical interactions among centromeres in *C. albicans* (30-32). This study now reveals that despite substantial karyotypic changes, a conserved principle of genome organization exists in two yeast species, *C. albicans* and *C. tropicalis,* with diverged centromere features.

Centromere and telomere proximal loci are hotspots for complex translocations

Using the chromosome-level assemblies of *C. tropicalis* type strain MYA-3404 and *C. albicans* type strain SC5314 (ASM18296v3), we performed a detailed genome-wide synteny analysis employing four different approaches. We used two analytical tools, Symap (33) and Satsuma synteny (34), and a custom approach to

287 identify the ICSBs based on the synteny of the conserved orthologs (Figure 3A).
288 Next, we compared and validated the results obtained from our custom approach of
289 analysis with another published tool Synchro (35). Considering the *C. albicans*
290 genome as the reference, all four methods of analyses suggest that six out of seven
291 centromeres (except *CEN6*) of *C. tropicalis* are located proximal to multiple ICSBs
292 (Figure 3A, S8A). Although it appears that *CtCEN6* escaped inter-centromeric
293 translocations, synteny analysis suggested that a chromosomal region carrying three
294 consecutive *CtCEN6*-proximal ORFs was lost in the *C. albicans* genome (Figure
295 S8B). Strikingly, these ICSBs are rare at the chromosomal arms (Figure 3A). ORF-
296 level synteny analysis further revealed that four out of seven centromeres (*CEN2*,
297 *CEN3*, *CEN5*, and *CENR*) in *C. tropicalis* are precisely located at the ICSBs (Figure
298 S8C), while multiple ICSBs are located within ~100 kb of other two centromeres
299 (Figure 3A). Additionally, a convergence of orthoblocks from as many as four
300 different chromosomes of *C. albicans* was detected within 100 kb of *C. tropicalis*
301 centromeres (Figure 3B). It is important to note that by using the *C. tropicalis*
302 genome as the reference, all centromeres of *C. albicans*, except *CaCEN2*, were
303 found to be associated with ICSBs (Figure S8D). Taken together, centromeres of
304 both these species are found to be associated with chromosomal translocations.
305
306 To correlate the frequency of translocations with the spatial genome
307 organization, we quantified ICSB density (the number of ICSBs per 100 kb of the
308 genome) for different zones across the chromosome for all chromosomes except
309 CtChr6 (Figure 3C). Our analysis reveals that the ICSB density is maximum at the
310 centromere-proximal zones for all six chromosomes, but drops sharply at the
311 chromosomal arms. However, the ICSB density near the telomere-proximal zone for
312 Chr2, Chr4, and ChrR shows an increase compared to the chromosomal arms, albeit
313 at a lower magnitude than centromeres. We also compared the lengths of
314 orthoblocks across three different genomic zones - the centromere-proximal (0 - 300
315 kb from the centromere on both sides), centromere-distal (>300 kb from the
316 centromere to 200 kb away from the telomere ends), and telomere-proximal (0 - 200
317 kb from the telomere ends) zones. This analysis further reveals that the lengths of
318 the orthoblocks located proximal to centromeres and telomeres are significantly
319 smaller than orthoblocks located at the centromere-/telomere-distal zones (Figure
320 3D).

321

322 We further probed into the consequences of strong inter-centromeric
323 interactions, as described above. Synteny analysis across centromere-proximal
324 regions of the two species hints that inter-centromeric translocations may have
325 occurred in the common ancestor of *C. albicans* and *C. tropicalis*. If such is the case,
326 the centromere-proximal ORFs of different chromosomes in *C. tropicalis* should have
327 converged on the *C. albicans* genome. Indeed, we identified at least ten loci where a
328 convergence of *C. tropicalis* ORFs from different chromosomes had taken place in
329 *C. albicans* (Figure S8E). Intriguingly, we found four such loci that are proximal to the
330 centromeres (*CEN3*, *CEN4*, *CEN7*, and *CENR*) in *C. albicans* (Figure 3E-F, S8F-G).
331 This observation strongly supports the possibility of inter-centromeric translocation
332 events in the common ancestor of *C. albicans* and *C. tropicalis.* Additionally, the
333 other four centromeres in *C. albicans* are located proximal to ORFs, orthologs of
334 which are also proximal to the centromeres in *C. tropicalis* (Figure S8E). We posit
335 that the ancestral HIR-associated centromeres were lost in *C. albicans,* and ENCs
336 formed proximal to the ancestral centromere loci on unique DNA sequences. A
337 similar centromere type transition within two isolates of *C. parapsilosis,* another
338 species of the CUG-Ser1 clade, has been recently reported (36).
339

340 **Rapid transition in the centromere type within the members of the CUG-Ser1**
341 **clade**

342 Since multiple translocation events near centromeric regions of the *C.*
343 *tropicalis* genome could be detected, we hypothesized that complex translocations
344 between HIR-associated centromeres in the common ancestor of *C. albicans* and *C.*
345 *tropicalis* led to the loss of HIR and the evolution of unique centromere types
346 observed in *C. albicans* and *C. dubliniensis.* However, the genomic rearrangements
347 are rare events, even at the evolutionary time scale. Therefore, if HIR-associated
348 centromeres are to be the ancestral state from which unique centromeres were
349 derived, some other closely related species should have retained HIR-associated
350 centromeres. Indeed, we identified eight HIR-associated structures (Table S7), in the
351 reference genome of *C. parapsilosis* strain CDC317 (ASM18276v2). Identification of
352 the HIR-associated structures present at the intergenic and transcription-poor
353 regions, one each on all eight chromosomes, suggests that these loci are the
354 putative centromeres of *C. parapsilosis*. Indeed, it was recently reported that all eight

355 CENP-A^{Cse4} enriched centromeres in the CLIB214 strain of *C. parapsilosis* are
356 located at HIR-associated loci (36). Based on these lines of evidence, we conclude
357 that the common ancestor of *C. albicans* and *C. tropicalis* possibly carried HIR-
358 associated centromeres. Surprisingly, two centromeres in another isolate (90-137) of
359 *C. parapsilosis* have been shown to be formed on non-HIR-associated loci (36).
360 However, the driving force triggering polymorphisms in centromere locations within
361 the same species is yet to be understood.
362
363 Although IRs are present in *CEN4*, *CEN5*, and *CENR* of *C. albicans,* these
364 sequences are not homogenized like the HIR-associated centromeres in *C. tropicalis*
365 (Figure 4A). To study the presence of HIRs in *C. sojae* (NCYC-2607), a sister
366 species of *C. tropicalis* (23), we assembled its genome into 42 contigs, including
367 seven chromosome-length contigs (Methods). Using this assembly, we identified
368 seven putative centromeres in *C. sojae* as intergenic and HIR-associated loci
369 syntenic to the centromeres in *C. tropicalis* (Figure S9A-B, D). Each of these seven
370 putative centromeres in *C. sojae* consists of a ~2 kb long CC region flanked by 3-12
371 kb long inverted repeats (Table S5). Using a similar approach, we identified six HIR-
372 associated centromeres in the publicly available genome assembly (ASM332773v1)
373 of *Candida viswanathii*, another species closely related to *C. tropicalis* (Figure S9C,
374 E, Table S6) (37). A dot-plot analysis identified the presence of homologous
375 sequences shared across IRs but not among the CC elements (Figure 4A) of the
376 HIR-associated centromeres present in *C. tropicalis* and the putative centromeres of
377 *C. sojae* and *C. viswanathii* (Table S7). Moreover, we detected extensive structural
378 conservation in centromere DNA elements, especially among IRs within an individual
379 species (Figure S10A). These structural feature of IRs are also significantly
380 conserved across the three species, *C. tropicalis*, *C. sojae,* and *C. viswanathii*
381 (Figure S10B).
382
383 Cloning of a full-length centromere of *C. tropicalis* in a replicative plasmid
384 facilitated *de novo* CENP-A^{Cse4} deposition but failed to do so when the native IRs
385 were replaced with Ca*CEN5* IRs (21). This result indicated DNA sequence specificity
386 is required for centromere function in *C. tropicalis.* To identify the DNA sequence as
387 a putative genetic element, we analyzed centromere DNA sequences of all three
388 *Candida* species with HIR-associated centromeres and the unique centromeres of *C.*

389 *albicans* for the presence of any conserved motif(s) (Methods). This analysis
390 identified a highly conserved 12-bp motif (dubbed as IR-motif) (Figure 4B) clustered
391 specifically at centromeres but not anywhere else in the entire genome of *C.*
392 *tropicalis, C. sojae* and *C. viswanathii* (Figure 4C-D, S10C). On the contrary, the IR-
393 motif density at centromeres in *C. albicans* remains approximately an order of
394 magnitude lower than that of *C. tropicalis* (Figure 4C). This observation indicates a
395 potential function of IR-motifs in the regulation of *de novo* CENP-A^{Cse4} loading in *C.*
396 *tropicalis*. Moreover, this *CEN*-enriched motif found at IRs is absent at central core
397 region in *C. tropicalis* (Figure 4E) and at the putative centromeres in *C. sojae* and *C.*
398 *viswanathii* (Figure S10D). Additionally, we noted that the direction of the IR-motif is
399 diverging away from the central core in *C. tropicalis* (Figure S10E**)** as well as in the
400 other two species (Figure S10F). The conserved structure and organization of the
401 IR-motif sequences in the HIR-associated centromeres of three *Candida* species
402 suggest an inter-species conserved function of the IR DNA sequence. However, the
403 clusters of IR-motifs are located at a variable distance from CC in these species
404 (Figure S10G). The importance of the sequence and the density of IR-motifs on the
405 centromere function is yet to be determined.
406
407 **Discussion**
408
409 In this study, we improved the current genome assembly of the human fungal
410 pathogen *C. tropicalis* by employing SMRT-seq, 3C-seq, and chromoblot
411 experiments, and present Assembly2020, the first chromosome-level gapless
412 genome assembly of this organism. We further identified three large-scale
413 duplication events and few small-scale CNV loci in its genome, phased the diploid
414 genome of *C. tropicalis*, and mapped SNPs and indels. We constructed a genome-
415 wide chromatin contact map and identified significant centromere-centromere as well
416 as telomere-telomere spatial interactions. Comparative genome analysis between *C.*
417 *albicans* and *C. tropicalis* reveals that six out of seven centromeres of *C. tropicalis*
418 are mapped precisely at or proximal to ICSBs. Strikingly, ORFs proximal to the
419 centromeres of *C. tropicalis* are converged into specific regions on the *C. albicans*
420 genome, suggesting that inter-centromeric translocations may have occurred in their
421 common ancestor. Moreover, the presence of HIR-associated putative centromeres
422 in *C. sojae* and *C. viswanathii,* like in *C. tropicalis*, suggests that such a centromere

423 structure is plausibly the ancestral form in the CUG-Ser1 clade but lost both in *C.*
424 *albicans* and *C. dubliniensis.* We propose that loss of such a centromere structure
425 might have occurred during translocation events involving centromeres of
426 homologous DNA sequences in the common ancestor, to give rise to ENCs on
427 unique DNA sequences and facilitated speciation.
428
429 Unlike other centromeres, *CEN6* of *C. tropicalis* did not seem to undergo
430 inter-centromeric translocations. A closer analysis revealed that three *CEN6*-
431 associated ORFs of *C. tropicalis* are absent in the *C. albicans* genome while the
432 other flanking ORFs remain conserved. This observation can be explained by a
433 double-stranded DNA break at the centromere followed by the fusion of broken ends
434 resulting in the loss of those ORFs.
435
436 The availability of the chromosome-level genome assembly and improved
437 annotations of genomic variants and genes absent in the publicly available
438 fragmented genome assembly of *C. tropicalis* should greatly facilitate genome-wide
439 association studies to understand the pathobiology of this organism including the
440 cause of antifungal drug resistance. Besides, this study sheds light on how genetic
441 elements required for *de novo* centromere establishment in an ancestral species
442 could be lost in the derived lineages to give rise to epigenetically-regulated
443 centromeres.
444
445 *C. tropicalis* is a human pathogenic ascomycete, closely related to the well-
446 studied model fungal pathogen *C. albicans* (38). These two species diverged from
447 their common ancestor ~39 million years ago (39) and evolved with distinct
448 karyotypes (21), having different phenotypic traits (40), and ecological niches (41).
449 While *C. albicans* remains the primary cause of candidiasis worldwide, systemic
450 ICU-acquired candidiasis is primarily (30.5-41.6%) caused by *C. tropicalis* in tropical
451 countries including India (42), Pakistan (43), and Brazil (44). Moreover, the
452 occurrence of drug resistance, particularly multidrug resistance, in *C. tropicalis* is on
453 the rise (42, 45, 46). Therefore, relatively less-studied *C. tropicalis* is emerging as a
454 major threat for nosocomial candidemia with 29-72% broad spectrum mortality rate
455 (47). Fluconazole resistance in *C. albicans* can be gained due to segmental
456 aneuploidy of Chr5 containing long IRs at the centromere, by the formation of

457 isochromosomes (48), which was also identified in Chr4 with IRs at its centromere
458 (49). All seven centromeres in *C. tropicalis* are associated with long IRs with the
459 potential to form isochromosomes.
460
461 Since the mechanism of homology search during HR is positively influenced
462 by spatial proximity and the extent of DNA sequence homology (3, 50), at least in the
463 engineered model systems, it is expected that spatially clustered homologous DNA
464 sequences undergo more translocation events than other loci. Although these factors
465 were not shown to be involved in karyotypic rearrangements during speciation, a
466 retrospective survey in light of spatial proximity and homology now offers a better
467 explanation. For example, the bipolar to the tetrapolar transition of the mating type
468 locus in the *Cryptococcus* species complex was associated with inter-centromeric
469 recombination following pericentric inversion (51). Similar inter-centromeric
470 recombination has been reported in the common ancestor of two fission yeast
471 species, *Schizosaccharomyces cryophilus* and *Schizosaccharomyces octosporus*
472 (16). These examples raise an intriguing notion that centromeres serve as sites of
473 recombination, which may lead to centromere loss and/or the emergence of ENCs.
474 This notion is supported by the fact that DSBs at centromeres following fusion of the
475 acentric fragments to other chromosomes led to chromosome number reduction in
476 *Ashbya* species (15) and *Malassezia* species (52). Genomic instability at the
477 centromere can also lead to fluconazole resistance, as in the case of
478 isochromosome formation on Chr5 of *C. albicans* (48). Additionally, breaks at the
479 centromeres were reported to be associated with cancers in humans (53).
480
481 What would be the consequence of the spatial proximity of chromosomal
482 regions with high DNA sequence homology in other domains of life? Inter-
483 chromosomal contacts between chromosome pairs have been correlated with the
484 number of translocation events in both naturally occurring populations and
485 experimentally induced mammalian cells (54-63). It has been suggested that
486 contacts between various chromosomal territories as well as their relative positions
487 in the nucleus influence the sites and frequency of translocation events both in flies
488 and mammals (58, 64-68). While centromeres remained clustered either throughout
489 the cell cycle or most parts of it in many fungal species, such is not the case in
490 metazoan cells. Nevertheless, one of the well-studied translocation events,

491 Robertsonian translocation (RT) involving fusion between arms of two different
492 chromosomes near a centromere, is the most frequently detected chromosomal
493 abnormality in humans (69). The occurrence of RT was first reported in
494 grasshoppers (70) and subsequently it has been implicated in the karyotype
495 evolution in humans (69), mice (71, 72), and wheat (73). Moreover, RTs cause
496 sterility in humans (74), often linked with the heterogeneity of carcinomas (75), and
497 implicated in genetic disorders (76). Intriguingly, cytological and Hi-C based
498 evidence (77) of spatial proximity (reviewed in (6)) among the repeat-associated
499 centromere DNA sequences (78) in these species supports a possibility that RTs
500 may have been guided by spatial proximity. Similarly, chromoplexy, involving a
501 series of translocation events among multiple chromosomes without alterations in
502 the copy number, was identified in prostate cancers (79, 80). Although fine mapping
503 of translocation events at the repetitive regions in human cancer cells is challenging,
504 the growing evidence that such events are associated with the formation of
505 micronuclei (81) supports the idea that the spatial genome organization may
506 influence chromoplexy as well (82).
507
508 The identification of HIR-associated putative centromeres in *C. parapsilosis*,
509 *C. sojae,* and *C. viswanathii* supports the idea that the unique centromeres might
510 have evolved from an ancestral HIR-associated centromere (83) (Figure 5A**).** While
511 HIR-associated centromeres of *C. tropicalis, C. sojae,* and *C. viswanathii* form on
512 different DNA sequences, a well-conserved IR-motif was identified in this study that
513 is present in multiple copies on the centromeric IR sequences across these three
514 species. Some centromeres in *C. albicans* carry chromosome-specific IRs but lack
515 IR-motifs. Besides, *CaCEN5* IRs could not functionally complement the centromere
516 function in *C. tropicalis* for the *de novo* CENP-A^{Cse4} recruitment. This indicates a
517 possible role of the conserved IR-motifs on species-specific centromere function
518 (21). Therefore, the loss of HIR-associated centromeres in *C. albicans* that are only
519 epigenetically propagated (22) clearly shows how the ability of *de novo*
520 establishment of kinetochore assembly in an ancestral lineage can be lost in a
521 derived lineage. However, the mechanism through which IR-motifs may regulate
522 centromere identity remains to be explored.
523

524 Loss of HIR-associated centromeres during inter-centromeric translocations
525 or MIR must have been catastrophic for the cell, and the survivor was obligated to
526 activate another centromere at an alternative locus. How is such a location
527 determined? Artificial removal of a native centromere in *C. albicans* leads to the
528 activation of a neocentromere (84, 85), which then becomes part of the centromere
529 cluster (30). This evidence supports the existence of a spatial determinant, known as
530 the CENP-A cloud or CENP-A-rich zone (84, 86), influencing the preferential
531 formation of neocentromere at loci proximal to the native centromere (84, 87). We
532 found that the unique and different centromeres of *C. albicans* are located proximal
533 to the ORFs, which are also proximal to the centromeres in *C. tropicalis*. This
534 observation indicates that the formation of the new centromeres in *C. albicans* may
535 have been influenced by spatial proximity to the ancestral centromere cluster.
536 However, new centromeres of *C. albicans* are formed on loci with completely unique
537 and different DNA sequences. Similar to centromeres of *C. albicans,* centromere
538 repositioning events may lead to the formation of ENCs, which are often associated
539 with speciation in mammals (88, 89). It was found that the location of one
540 centromere in horse varies across individuals (90, 91). Although, there are cases
541 where ENCs formed without genomic rearrangements, the driving force facilitating
542 centromere relocation was proposed to be associated with chromosomal inversion
543 and translocation in certain cases (92). Because of these reasons, it may be logical
544 to consider the centromeres of *C. albicans* as ENCs (Figure 5B). Intriguingly, even
545 after the catastrophic chromosomal rearrangements, the ENCs in *C. albicans* remain
546 clustered similar to *C. tropicalis* (Figure 5C). This observation identifies spatial
547 clustering of centromeres as a matter of cardinal importance for the fungal genome
548 organization.
549
550 **Methods**
551 The strains, primers, and plasmids used in this study are listed in SI Appendix,
552 Tables S8, S9, and S10, respectively. Details of all of the experimental procedures
553 and data analysis are given in SI Methods. All sequencing data reported in the study
554 and the genome assembly of *C. tropicalis* and *C. sojae* have been submitted to NCBI
555 under the BioProject accession numbers PRJNA596050 and PRJNA604451.
556
557 **Acknowledgments**

558 We thank all the members of KS laboratory and AS laboratory for stimulating
559 discussions and critical reading of the manuscript. We acknowledge S. Sun and J.
560 Heitman for helping with SMRT-seq of *C. tropicalis* at the PacBio sequencing facility
561 at Duke University. We also thank A.I.S. Khalil for helping with CNAtra software for
562 CNV analysis. Illumina sequencing experiments for the *C. sojae* genome were
563 performed at Clevergene Biocorp, Bangalore, India. We also thank B. Suma for
564 confocal microscopy, JNCASR. K.G. acknowledges Shyama Prasad Mukherjee
565 Fellowship from Council of Scientific and Industrial Research (CSIR), Govt. of India
566 [07/733(0181)/2013-EMR-I] and financial assistance from JNCASR. This project is
567 supported by a grant (BT/PR27490/Med/29/1323/2018) from the Department of
568 Biotechnology (DBT), Govt. of India to K.S. K.S. acknowledges TATA innovation
569 fellowship (BT/HRD/35/01/03/2017) and Department of Biotechnology grant in Life
570 Science Research, Education and Training at JNCASR (BT/INF/22/SP27679/2018).
571 Intramural funding from JNCASR is acknowledged. This work is also supported by
572 Nanyang Technological University's Nanyang Assistant Professorship grant and
573 Singapore Ministry of Education Academic Research Fund Tier 1 grant [RG39/18] to
574 A.S.
575

576 **Author contributions**

577 K.S. and A.S. supervised the study. K.S., A.S., K.G., and Y.C. conceived the idea
578 and designed the experiments. K.G. performed N-gap filling, haplotype analysis,
579 genome-wide synteny analyses, identification of the putative HIR-associated
580 centromeres motif analysis, chromoblot analysis, Southern blotting, and subcellular
581 localization experiments, Oxford Nanopore library preparation for *C. sojae* and
582 generated its genome assembly. Y.C. analyzed 3C-seq data of *C. tropicalis* for
583 chromatin contact map generation, aggregate signal analysis, and statistical
584 comparison between telomeric interactions and bulk chromatin. With 3C-seq data
585 YC validated joining of contigs and identified the CNVs in *the C. tropicalis* genome.
586 B.C.T. and K.G. performed SMIS and Canu run, the scaffolding of telomeres, and
587 Pilon polishing. R.M. and K.G. constructed aneuploid strains. S.R.B.M.M. performed
588 the 3C-seq library preparation. C.O.B. and G.B. performed scaffolding of *C. tropicalis*
589 genome in 16 contigs (Assembly B). K.G., K.S., Y.C., and A.S. wrote the manuscript
590 and incorporated inputs from all of the authors. K.S. and A.S. edited the manuscript
591 and provided the funding.

592

593 **Conflict of Interests**

594 The authors declare that they have no conflict of interest.

595

596 **Figure legends**

597

598 **Figure 1. Construction of the gapless assembly of *C. tropicalis* type strain**
599 **MYA-3404 in seven chromosomes.**

600 A. Schematic showing the stepwise construction of the gapless chromosome-level
601 assembly (Assembly2020) of *C. tropicalis* (also see Figure S1 and S2). B. An
602 ethidium bromide (EtBr)-stained CHEF gel image of separated chromosomes of the
603 *C. tropicalis* (strain MYA-3404) and *C. albicans* (strain SC5314) (Methods). *C.*
604 *albicans* chromosomes are used as size markers for estimation and validation of
605 lengths and identities of *C. tropicalis* chromosomes in the newly constructed
606 Assembly2020. C. An ideogram of seven chromosomes of *C. tropicalis* as deduced
607 from Assembly2020 and drawn to scale. The genomic location of the three loci
608 showing copy number variations (CNVs), *DUP4, DUP5* and *DUPR* located on Chr4,
609 Chr5 and ChrR respectively, are marked and depicted as striped box. The CNVs for
610 which the correct homolog-wise distribution of the duplicated copy is unknown are
611 marked with asterisks. Homolog-specific differences for Chr1 and Chr4, occurred
612 due to an exchange of chromosomal parts in a balanced heterozygous translocation
613 between Chr1B and Chr4B, are highlighted with black borders (also see Figure
614 S4C). D. A circos plot showing the genome-wide distribution of various sequence
615 features. Very high sequence coverage at rDNA locus is clipped for more precise
616 representation and marked with an asterisk.

617

618 **Figure 2. Spatial genome organization reveals centromere-centromere and**
619 **telomere-telomere contacts in *C. tropicalis.***

620 A. A representative field image of *C. tropicalis* (strain CtKS102) cells expressing
621 Protein-A tagged CENP-A^{Cse4}. CENP-A signals (blue) were obtained using anti-
622 Protein A antibodies by indirect immuno-fluorescence microscopy. Nuclei of the
623 corresponding cells were stained by DAPI (blue). The images were acquired using a
624 DeltaVision imaging system (GE) and processed using FIJI software (93). Scale, 2
625 μm. B. A 3D reconstruction showing clustered kinetochores marked by CENP-A^{Cse4}

626 (red) at the periphery of the DAPI-stained nucleus (blue) using Imaris software
627 (Oxford Instruments) in *C. tropicalis*. Scale, 2 μm. C. A genome-wide contact
628 probability heatmap (bin size = 10 kb) generated using 3C-seq data. Chromosome
629 labels and their corresponding ideograms are shown on the axes of the heatmap.
630 Colorbar represents the contact probability in the log2 scale. D. Zoom in view of
631 heatmap showing Chr4 and Chr5 from panel C (blue box). E. Heatmaps plotted from
632 aggregate signal analysis of matrices (bin size = 2 kb) surrounding centromere-
633 centromere (top) or telomere-telomere interactions (bottom). *Top*, genomic loci
634 containing mid-points of centromeres are aligned at the center (red bar); *bottom*,
635 genomic loci from 5′ or 3′ ends of chromosomes are aligned at the bottom right
636 corner.
637
638 **Figure 3. Genome-wide mapping of interchromosomal synteny breakpoints in**
639 ***C. tropicalis* identifies a spatial cue for karyotype evolution.**
640 A. Scaled representation of the color-coded orthoblocks (relative to *C. albicans*
641 chromosomes) and ICSBs (white lines) in *C. tropicalis* (Methods). Orthoblocks are
642 defined as stretches of the target genome (*C. tropicalis*) carrying more than two
643 syntenic ORFs from the same chromosome of the reference genome (*C. albicans*).
644 The centromeres are represented with black arrowheads. B. Zoom in view of the *C.*
645 *tropicalis* centromere-specific ICSBs on *CEN2*, *CEN3*, *CEN5* and *CENR* showing the
646 color-coded (relative to *C. albicans* chromosomes) ORFs flanking each centromere.
647 *C. tropicalis*-specific unique ORFs proximal to *CEN3* and *CEN5* are shown in red. C.
648 A plot showing the chromosome-wise ICSB density, calculated as number of ICSBs
649 per 100 kb of the C. *tropicalis* genome (*y*-axis), as a function of the linear distance
650 from the centromere in nine bins. These bins are a) 0 - 100 kb on both sides of
651 centromere (bin I), b) 100 - 200 kb (bin II), c) 200 - 300 kb (bin III), d) 300 - 400 kb
652 (bin IV), e) 400 - 500 kb (bin V), f) 500 - 600 kb (bin VI), g) 600 - 700 kb (bin VII), h)
653 >700 kb to 200 kb from telomere ends (bin VIII), and i) 200 kb from the telomere
654 ends (bin IX). Chr6 was excluded from this analysis, as it does not harbor any ICSB.
655 D. A violin plot comparing the distribution of lengths of orthoblocks (*y*-axis) at three
656 different genomic zones: a) the centromere-proximal zone (CP), b) the centromere-
657 distal zone (CD), and c) telomere-proximal zone (TP). Orthoblocks, which span over
658 more than one zone, were assigned to the zone with maximum overlap. The
659 centromere-distal dataset was compared with the other two groups using the Mann-

660 Whitney U test and the respective *P* values are mentioned. E - F. Circos plots
661 representing the convergence of centromere-proximal ORFs of *C. tropicalis*
662 chromosomes near the centromeres (*CEN4* and *CEN7*) of *C. albicans*.
663 Chromosomes of *C. tropicalis* and *C. albicans* are marked with black and purple
664 filled circles at the beginning of each chromosome, respectively.
665
666 **Figure 4. Genome-wide analysis of centromere DNA sequences across the**
667 **CUG-Ser1 clade reveals the emergence of unique centromeres from an**
668 **ancestral homogenized inverted repeat-associated centromere type.**
669 A. A dot-plot matrix representing the sequence and structural homology among
670 species of the CUG-Ser1 clade was generated using Gepard (Methods). B. A logo
671 plot showing the 12 bp-long IR-motif, identified using MEME-suit (Methods). C. The
672 distribution of IR-motif density on centromere DNA sequences and across the entire
673 genome of each species was calculated as the number of motifs per kb of DNA
674 (Methods). Note that *C. albicans* and *C. dubliniensis* centromeres that form on
675 unique and different DNA sequences do not contain the IR-motif. D. IGV track
676 images showing the IR-motif density across seven chromosomes of *C. tropicalis.*
677 The location of the centromere on each chromosome is marked with a black
678 arrowhead. E. IGV track images showing the IR-motif distribution across seven HIR-
679 associated centromeres of *C. tropicalis.*
680
681 **Figure 5. The spatial genome organization remained conserved in the CUG-**
682 **Ser1 clade despite centromere type diversity.**
683 A. A maximum likelihood-based phylogenetic tree of closely related CUG-Ser1
684 species analyzed in this study. The centromere structure of each species is shown
685 and drawn to scale. B. A model showing possible events during the loss of HIR-
686 associated centromeres and emergence of the unique centromere type through
687 inter-centromeric translocations possibly occurred in the common ancestor of *C.*
688 *tropicalis* and *C. albicans.* The model is drawn to show translocation events involving
689 two *C. tropicalis* chromosomes (CtChr3 and CtChr4) as representatives, which can
690 be mapped proximal to the centromere on *C. albicans* ChrR (CaChrR) as shown in
691 Figure 3F. C. Rabl-like chromosomal conformation is maintained despite inter-
692 centromeric translocations that facilitated centromere type transition.
693

1. Searle JB (1998) Speciation, chromosomes, and genomes. *Genome Research* 8(1):1-3.
2. Lee CS*, et al.* (2016) Chromosome position determines the success of double-strand break repair. *Proceedings of the National Academy of Sciences of the United States of America* 113(2):E146-154.
3. Agmon N, Liefshitz B, Zimmer C, Fabre E, & Kupiec M (2013) Effect of nuclear architecture on the efficiency of double-strand break repair. *Nat Cell Biol* 15(6):694-699.
4. Burgess SM & Kleckner N (1999) Collisions between yeast chromosomal loci in vivo are governed by three layers of organization. *Genes Dev* 13(14):1871-1883.
5. Piazza A, Wright WD, & Heyer WD (2017) Multi-invasions are recombination byproducts that induce chromosomal rearrangements. *Cell* 170(4):760-773 e715.
6. Muller H, Gil J, Jr., & Drinnenberg IA (2019) The impact of centromeres on spatial genome architecture. *Trends Genet* 35(8):565-578.
7. Clarke L & Carbon J (1980) Isolation of a yeast centromere and construction of functional small circular chromosomes. *Nature* 287(5782):504-509.
8. Mahtani MM & Willard HF (1990) Pulsed-field gel analysis of α-satellite DNA at the human X chromosome centromere: high-frequency polymorphisms and array size estimate. *Genomics* 7(4):607-613.
9. Navarro-Mendoza MI*, et al.* (2019) Early diverging fungus *Mucor circinelloides* lacks centromeric histone CENP-A and displays a mosaic of point and regional centromeres. *Curr Biol* 29(22):3791-3802 e3796.
10. Meraldi P, McAinsh AD, Rheinbay E, & Sorger PK (2006) Phylogenetic and structural analysis of centromeric DNA and kinetochore proteins. *Genome Biol* 7(3):R23.
11. Tromer EC, van Hooff JJE, Kops G, & Snel B (2019) Mosaic origin of the eukaryotic kinetochore. *Proceedings of the National Academy of Sciences of the United States of America* 116(26):12873-12882.
12. van Hooff JJ, Tromer E, van Wijk LM, Snel B, & Kops GJ (2017) Evolutionary dynamics of the kinetochore network in eukaryotes as revealed by comparative genomics. *EMBO Reports* 18(9):1559-1571.
13. Ekwall K (2007) Epigenetic control of centromere behavior. *Annu Rev Genet* 41(1):63-81.
14. Clarke L & Baum MP (1990) Functional analysis of a centromere from fission yeast: a role for centromere-specific repeated DNA sequences. *Molecular and Cellular Biology* 10(5):1863-1872.
15. Gordon JL, Byrne KP, & Wolfe KH (2011) Mechanisms of chromosome number evolution in yeast. *PLoS Genet* 7(7):e1002190.
16. Tong P*, et al.* (2019) Interspecies conservation of organisation and function between nonhomologous regional centromeres. *Nature Communications* 10(1):2343.
17. Kobayashi N*, et al.* (2015) Discovery of an unconventional centromere in budding yeast redefines evolution of point centromeres. *Curr Biol* 25(15):2026-2033.
18. Sanyal K, Baum M, & Carbon J (2004) Centromeric DNA sequences in the pathogenic yeast *Candida albicans* are all different and unique. *Proceedings of the National Academy of Sciences of the United States of America* 101(31):11374-11379.
19. Padmanabhan S, Thakur J, Siddharthan R, & Sanyal K (2008) Rapid evolution of Cse4p-rich centromeric DNA sequences in closely related pathogenic yeasts, *Candida albicans* and *Candida dubliniensis*. *Proceedings of the National Academy of Sciences of the United States of America* 105(50):19797-19802.

20. Kapoor S, Zhu L, Froyd C, Liu T, & Rusche LN (2015) Regional centromeres in the yeast *Candida lusitaniae* lack pericentromeric heterochromatin. *Proceedings of the National Academy of Sciences of the United States of America* 112(39):12139-12144.
21. Chatterjee G*, et al.* (2016) Repeat-associated fission yeast-like regional centromeres in the ascomycetous budding yeast *Candida tropicalis*. *PLoS Genet* 12(2):e1005839.
22. Baum M SK, Mishra PK, Thaler N, Carbon J. (2006) Formation of functional centromeric chromatin is specified epigenetically in *Candida albicans*. *Proceedings of the National Academy of Sciences* 103(40)(Oct 3):14877-14882.
23. Shen XX*, et al.* (2018) Tempo and mode of genome evolution in the budding yeast subphylum. *Cell* 175(6):1533-1545 e1520.
24. Butler G*, et al.* (2009) Evolution of pathogenicity and sexual reproduction in eight *Candida* genomes. *Nature* 459(7247):657-662.
25. Sexton T*, et al.* (2012) Three-dimensional folding and functional organization principles of the Drosophila genome. *Cell* 148(3):458-472.
26. Khalil AIS, Khyriem C, Chattopadhyay A, & Sanyal A (2020) Hierarchical discovery of large-scale and focal copy number alterations in low-coverage cancer genomes. *BMC Bioinformatics* 21(1):147.
27. Jones T*, et al.* (2004) The diploid genome sequence of *Candida albicans*. *Proceedings of the National Academy of Sciences of the United States of America* 101(19):7329-7334.
28. Duan Z*, et al.* (2010) A three-dimensional model of the yeast genome. *Nature* 465(7296):363-367.
29. Descorps-Declere S*, et al.* (2015) Genome-wide replication landscape of *Candida glabrata*. *BMC Biol* 13:69.
30. Burrack LS*, et al.* (2016) Neocentromeres provide chromosome segregation accuracy and centromere clustering to multiple loci along a *Candida albicans* chromosome. *PLoS Genet* 12(9):e1006317.
31. Sreekumar L*, et al.* (2019) Cis- and trans-chromosomal interactions define pericentric boundaries in the absence of conventional heterochromatin. *Genetics* 212(4):1121-1132.
32. Sreekumar L*, et al.* (2019) Orc4 spatiotemporally stabilizes centromeric chromatin. *bioRxiv*:465880, DOI: 465810.461101/465880.
33. Soderlund C, Bomhoff M, & Nelson WM (2011) SyMAP v3.4: a turnkey synteny system with application to plant genomes. *Nucleic Acids Res* 39(10):e68.
34. Grabherr MG RP, Meyer M, Mauceli E, Alföldi J, Di Palma F, Lindblad-Toh K. (2010) Genome-wide synteny through highly sensitive sequence alignment: Satsuma. *Bioinformatics.* 26(9):1145-1151.
35. Drillon G, Carbone A, & Fischer G (2014) SynChro: a fast and easy tool to reconstruct and visualize synteny blocks along eukaryotic chromosomes. *PLoS One* 9(3):e92621.
36. Ola M*, et al.* (2020) Polymorphic centromere locations in the pathogenic yeast Candida parapsilosis. *bioRxiv*:2020.2004.2009.034512.
37. Tsui CK, Daniel HM, Robert V, & Meyer W (2008) Re-examining the phylogeny of clinically relevant *Candida* species and allied genera based on multigene analyses. *FEMS Yeast Res* 8(4):651-659.
38. Legrand M, Jaitly P, Feri A, d'Enfert C, & Sanyal K (2019) *Candida albicans*: An emerging yeast model to study eukaryotic genome plasticity. *Trends Genet* 35(4):292-307.
39. Kumar S, Stecher G, Suleski M, & Hedges SB (2017) TimeTree: a resource for timelines, timetrees, and divergence times. *Mol Biol Evol* 34(7):1812-1819.

792 40. Cavalheiro M & Teixeira MC (2018) *Candida* Biofilms: threats, challenges, and
793 promising strategies. *Front Med (Lausanne)* 5:28.
794 41. Pappas PG, Lionakis MS, Arendrup MC, Ostrosky-Zeichner L, & Kullberg BJ (2018)
795 Invasive candidiasis. *Nat Rev Dis Primers* 4:18026.
796 42. Chakrabarti A*, et al.* (2015) Incidence, characteristics and outcome of ICU-acquired
797 candidemia in India. *Intensive Care Med* 41(2):285-295.
798 43. Farooqi JQ*, et al.* (2013) Invasive candidiasis in Pakistan: clinical characteristics,
799 species distribution and antifungal susceptibility. *J Med Microbiol* 62(Pt 2):259-268.
800 44. da Costa VG, Quesada RM, Abe AT, Furlaneto-Maia L, & Furlaneto MC (2014)
801 Nosocomial bloodstream *Candida* infections in a tertiary-care hospital in South
802 Brazil: a 4-year survey. *Mycopathologia* 178(3-4):243-250.
803 45. Xiao M*, et al.* (2015) Antifungal susceptibilities of *Candida glabrata* species
804 complex, *Candida krusei*, *Candida parapsilosis* species complex and *Candida*
805 *tropicalis* causing invasive candidiasis in China: 3 year national surveillance. *J*
806 *Antimicrob Chemother* 70(3):802-810.
807 46. Goncalves SS, Souza ACR, Chowdhary A, Meis JF, & Colombo AL (2016)
808 Epidemiology and molecular mechanisms of antifungal resistance in *Candida* and
809 *Aspergillus*. *Mycoses* 59(4):198-219.
810 47. Lamoth F, Lockhart SR, Berkow EL, & Calandra T (2018) Changes in the
811 epidemiological landscape of invasive candidiasis. *J Antimicrob Chemother*
812 73(suppl_1):i4-i13.
813 48. Selmecki A, Forche A, & Berman J (2006) Aneuploidy and isochromosome
814 formation in drug-resistant *Candida albicans*. *Science* 313(5785):367-370.
815 49. Todd RT, Wikoff TD, Forche A, & Selmecki A (2019) Genome plasticity in *Candida*
816 *albicans* is driven by long repeat sequences. *Elife* 8:e45954.
817 50. Seeber A, Hauer MH, & Gasser SM (2018) Chromosome dynamics in response to
818 DNA damage. *Annu Rev Genet* 52(1):295-319.
819 51. Wolfe K*, et al.* (2017) Fungal genome and mating system transitions facilitated by
820 chromosomal translocations involving intercentromeric recombination. *PLOS Biology*
821 15(8):e2002527.
822 52. Sankaranarayanan SR*, et al.* (2020) Loss of centromere function drives karyotype
823 evolution in closely related *Malassezia* species. *eLife* 9:e53944.
824 53. Barra V & Fachinetti D (2018) The dark side of centromeres: types, causes and
825 consequences of structural abnormalities implicating centromeric DNA. *Nat Commun*
826 9(1):4340.
827 54. Arsuaga J*, et al.* (2004) Chromosome spatial clustering inferred from radiogenic
828 aberrations. *International journal of radiation biology* 80(7):507-515.
829 55. Bickmore WA & Teague P (2002) Influences of chromosome size, gene density and
830 nuclear position on the frequency of constitutional translocations in the human
831 population. *Chromosome research* 10(8):707-715.
832 56. Branco MR & Pombo A (2006) Intermingling of chromosome territories in interphase
833 suggests role in translocations and transcription-dependent associations. *PLoS biology*
834 4(5).
835 57. Canela A*, et al.* (2017) Genome organization drives chromosome fragility. *Cell*
836 170(3):507-521. e518.
837 58. Engreitz JM, Agarwala V, & Mirny LA (2012) Three-dimensional genome
838 architecture influences partner selection for chromosomal translocations in human
839 disease. *PloS one* 7(9).

59. Hlatky L, Sachs RK, Vazquez M, & Cornforth MN (2002) Radiation-induced chromosome aberrations: Insights gained from biophysical modeling. *Bioessays* 24(8):714-723.
60. Holley W, Mian I, Park S, Rydberg B, & Chatterjee A (2002) A model for interphase chromosomes and evaluation of radiation-induced aberrations. *Radiation research* 158(5):568-580.
61. Klein IA*, et al.* (2011) Translocation-capture sequencing reveals the extent and nature of chromosomal rearrangements in B lymphocytes. *Cell* 147(1):95-106.
62. Roukos V, Burman B, & Misteli T (2013) The cellular etiology of chromosome translocations. *Current Opinion in Cell Biology* 25(3):357-364.
63. Zhang Y*, et al.* (2012) Spatial organization of the mouse genome and its role in recurrent chromosomal translocations. *Cell* 148(5):908-921.
64. Aten JA*, et al.* (2004) Dynamics of DNA double-strand breaks revealed by clustering of damaged chromosome domains. *Science* 303(5654):92-95.
65. Foster HA*, et al.* (2013) Relative proximity of chromosome territories influences chromosome exchange partners in radiation-induced chromosome rearrangements in primary human bronchial epithelial cells. *Mutation Research/Genetic Toxicology and Environmental Mutagenesis* 756(1-2):66-77.
66. Savage JR (1998) A brief survey of aberration origin theories. *Mutation Research/Fundamental and Molecular Mechanisms of Mutagenesis* 404(1-2):139-147.
67. Savage JR (2000) Proximity matters. *Science* 290(5489):62-63.
68. Meaburn KJ (2016) Spatial genome organization and its emerging role as a potential diagnosis tool. *Frontiers in genetics* 7:134.
69. Therman E, Susman B, & Denniston C (1989) The nonrandom participation of human acrocentric chromosomes in Robertsonian translocations. *Annals of human genetics* 53(1):49-65.
70. Robertson WRB (1916) Chromosome studies. I. Taxonomic relationships shown in the chromosomes of *Tettigidae* and *Acrididae*: V-shaped chromosomes and their significance in *Acrididae*, *Locustidae*, and *Gryllidae*: chromosomes and variation. *Journal of Morphology* 27(2):179-331.
71. Castiglia R & Capanna E (2002) Chiasma repatterning across a chromosomal hybrid zone between chromosomal races of *Mus musculus domesticus*. *Genetica* 114(1):35-40.
72. Dumas D & Britton-Davidian J (2002) Chromosomal rearrangements and evolution of recombination: comparison of chiasma distribution patterns in standard and Robertsonian populations of the house mouse. *Genetics* 162(3):1355-1366.
73. Friebe B, Zhang P, Linc G, & Gill B (2005) Robertsonian translocations in wheat arise by centric misdivision of univalents at anaphase I and rejoining of broken centromeres during interkinesis of meiosis II. *Cytogenetic and genome research* 109(1-3):293-297.
74. Guichaoua M*, et al.* (1990) Infertility in human males with autosomal translocations: meiotic study of a 14; 22 Robertsonian translocation. *Human genetics* 86(2):162-166.
75. Hermsen M*, et al.* (2005) Centromeric chromosomal translocations show tissue-specific differences between squamous cell carcinomas and adenocarcinomas. *Oncogene* 24(9):1571-1579.
76. Mattei M, Souiah N, & Mattei J (1984) Chromosome 15 anomalies and the Prader-Willi syndrome: cytogenetic analysis. *Human genetics* 66(4):313-334.
77. Imakaev M*, et al.* (2012) Iterative correction of Hi-C data reveals hallmarks of chromosome organization. *Nat Methods* 9(10):999-1003.

78. Kalitsis P, Griffiths B, & Choo KA (2006) Mouse telocentric sequences reveal a high rate of homogenization and possible role in Robertsonian translocation. *Proceedings of the National Academy of Sciences* 103(23):8786-8791.
79. Zhang CZ, Leibowitz ML, & Pellman D (2013) Chromothripsis and beyond: rapid genome evolution from complex chromosomal rearrangements. *Genes Dev* 27(23):2513-2530.
80. Baca SC*, et al.* (2013) Punctuated evolution of prostate cancer genomes. *Cell* 153(3):666-677.
81. Crasta K*, et al.* (2012) DNA breaks and chromosome pulverization from errors in mitosis. *Nature* 482(7383):53-58.
82. Meaburn KJ, Misteli T, & Soutoglou E (2007) Spatial genome organization in the formation of chromosomal translocations. *Seminars in cancer biology*, (Elsevier), pp 80-90.
83. Coughlan AY, Hanson SJ, Byrne KP, & Wolfe KH (2016) Centromeres of the yeast *Komagataella phaffii* (*Pichia pastoris*) have a simple inverted-repeat structure. *Genome Biology and Evolution* 8(8):2482-2492.
84. Thakur J & Sanyal K (2013) Efficient neocentromere formation is suppressed by gene conversion to maintain centromere function at native physical chromosomal loci in *Candida albicans*. *Genome Res* 23(4):638-652.
85. Ketel C*, et al.* (2009) Neocentromeres form efficiently at multiple possible loci in *Candida albicans*. *PLoS Genet* 5(3):e1000400.
86. Fukagawa T & Earnshaw WC (2014) Neocentromeres. *Curr Biol* 24(19):R946-947.
87. Scott KC & Sullivan BA (2014) Neocentromeres: a place for everything and everything in its place. *Trends Genet* 30(2):66-74.
88. Rocchi M, Archidiacono N, Schempp W, Capozzi O, & Stanyon R (2012) Centromere repositioning in mammals. *Heredity* 108(1):59-67.
89. Stanyon R*, et al.* (2008) Primate chromosome evolution: ancestral karyotypes, marker order and neocentromeres. *Chromosome Research* 16(1):17-39.
90. Wade C*, et al.* (2009) Genome sequence, comparative analysis, and population genetics of the domestic horse. *Science* 326(5954):865-867.
91. Purgato S*, et al.* (2015) Centromere sliding on a mammalian chromosome. *Chromosoma* 124(2):277-287.
92. Schubert I (2018) What is behind “centromere repositioning”? *Chromosoma* 127(2):229-234.
93. Schindelin J*, et al.* (2012) Fiji: an open-source platform for biological-image analysis. *Nature methods* 9(7):676-682.

Figure 1

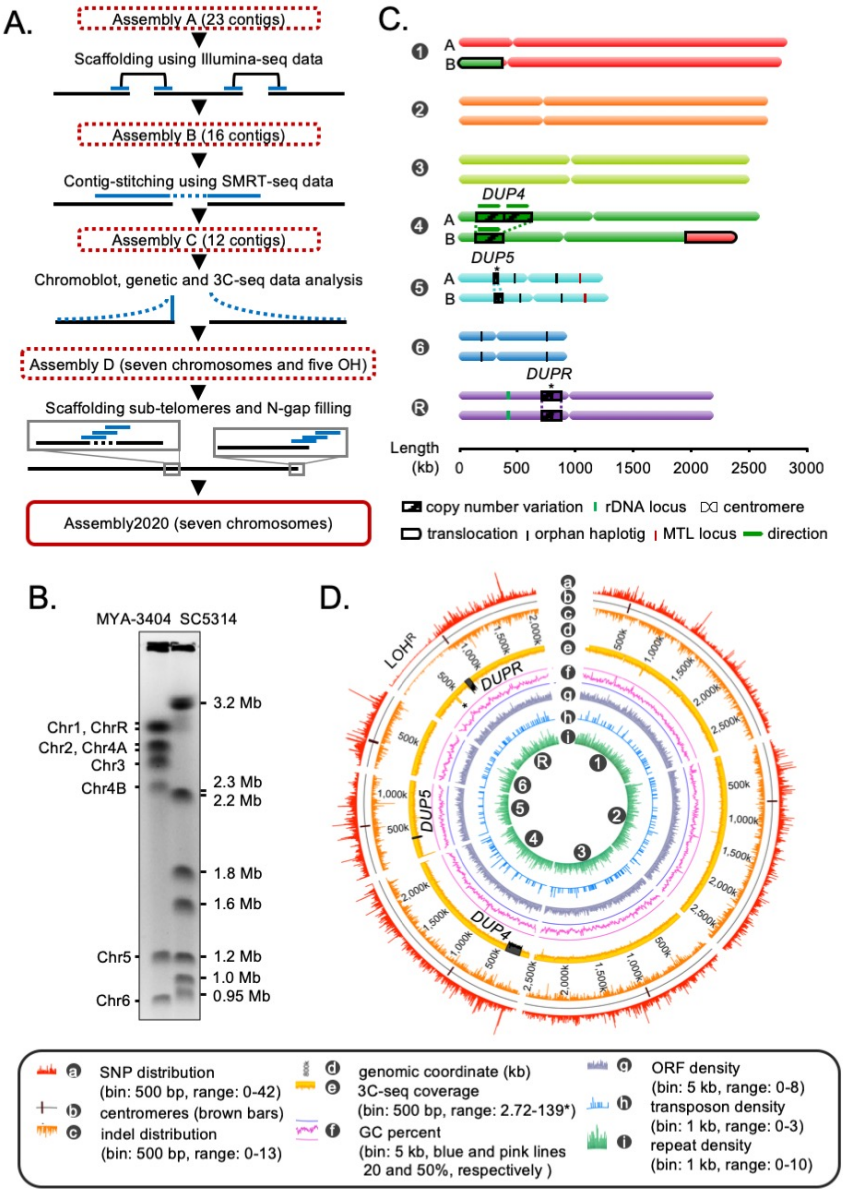
A.
Assembly A (23 contigs)
Scaffolding using Illumina-seq data
Assembly B (16 contigs)
Contig-stitching using SMRT-seq data
Assembly C (12 contigs)
Chromoblot, genetic and 3C-seq data analysis
Assembly D (seven chromosomes and five OH)
Scaffolding sub-telomeres and N-gap filling
Assembly2020 (seven chromosomes)
C.
DUP4
DUP5
DUPR
Length (kb)
0 500 1000 1500 2000 2500 3000
copy number variation
rDNA locus
centromere
translocation
orphan haplotig
MTL locus
direction
B.
MYA-3404 SC5314
Chr1, ChrR
Chr2, Chr4A
Chr3
Chr4B
Chr5
Chr6
3.2 Mb
2.3 Mb
2.2 Mb
1.8 Mb
1.6 Mb
1.2 Mb
1.0 Mb
0.95 Mb
D.
LOHR
DUPR
DUP5
DUP4
SNP distribution (bin: 500 bp, range: 0-42)
centromeres (brown bars)
indel distribution (bin: 500 bp, range: 0-13)
genomic coordinate (kb)
3C-seq coverage (bin: 500 bp, range: 2.72-139*)
GC percent (bin: 5 kb, blue and pink lines 20 and 50%, respectively)
ORF density (bin: 5 kb, range: 0-8)
transposon density (bin: 1 kb, range: 0-3)
repeat density (bin: 1 kb, range: 0-10)

Figure 2

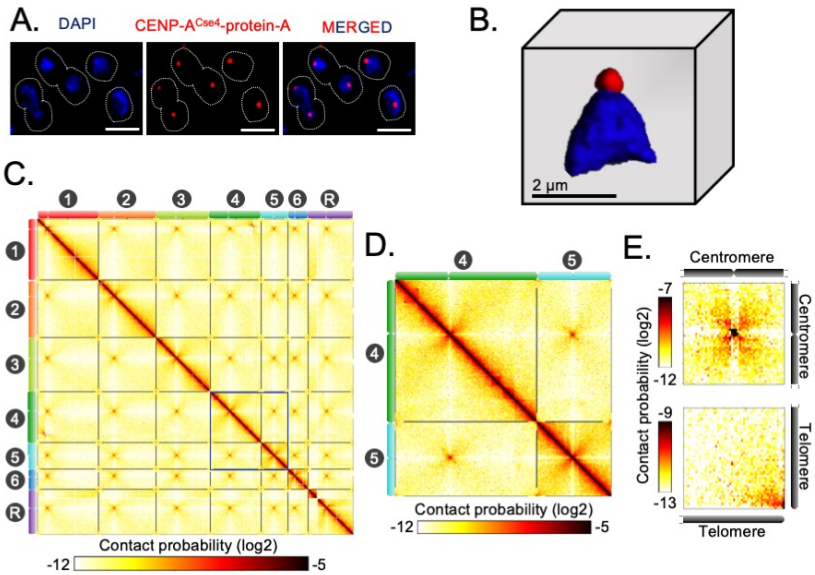
A.
DAPI
CENP-A^{Cse4}-protein-A
MERGED
B.
2 µm
C.
1 2 3 4 5 6 R
Contact probability (log2)
-12
-5
D.
4 5
Contact probability (log2)
-12
-5
E.
Centromere
Centromere
Telomere
Telomere
Contact probability (log2)
-7
-12
-9
-13

Figure 3

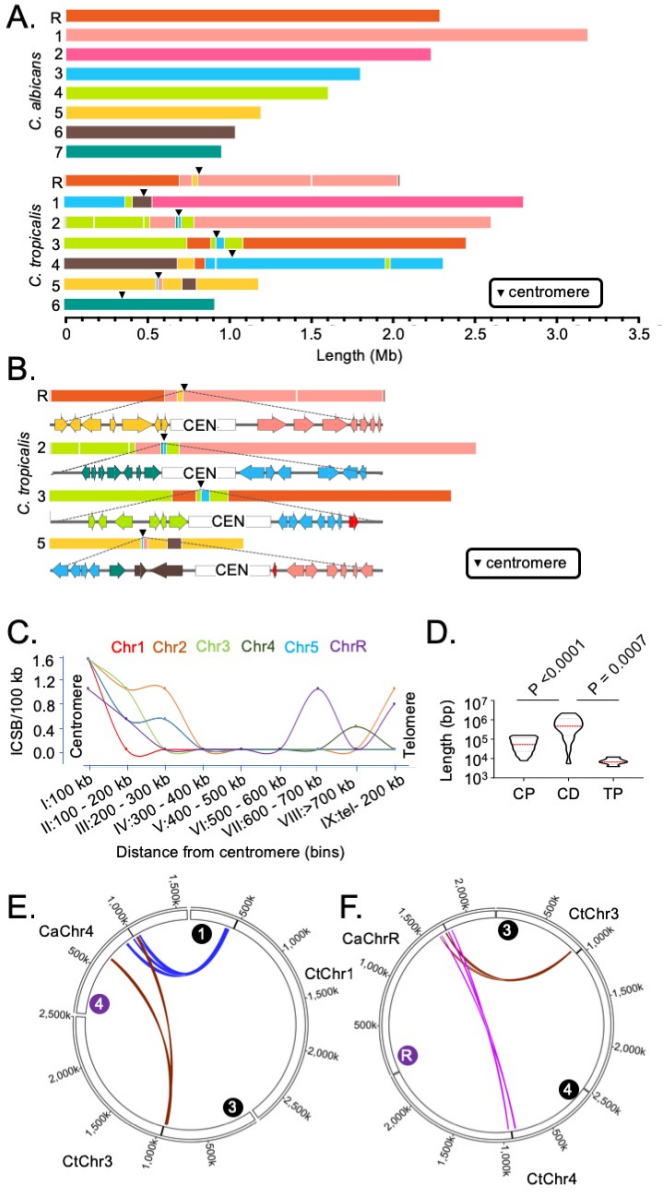
A.
C. albicans
R
1
2
3
4
5
6
7
C. tropicalis
R
1
2
3
4
5
6
centromere
0
0.5
1.0
1.5
2.0
2.5
3.0
3.5
Length (Mb)
B.
C. tropicalis
R
2
3
5
CEN
centromere
C.
Chr1 Chr2 Chr3 Chr4 Chr5 ChrR
ICSB/100 kb
1.6
1.2
0.8
0.4
0.0
Centromere
Telomere
I:100 kb
II:100 - 200 kb
III:200 - 300 kb
IV:300 - 400 kb
V:400 - 500 kb
VI:500 - 600 kb
VII:600 - 700 kb
VIII:>700 kb
IX:tel- 200 kb
Distance from centromere (bins)
D.
P <0.0001
P = 0.0007
Length (bp)
CP
CD
TP
E.
CaChr4
CtChr1
CtChr3
F.
CaChrR
CtChr3
CtChr4

Figure 4

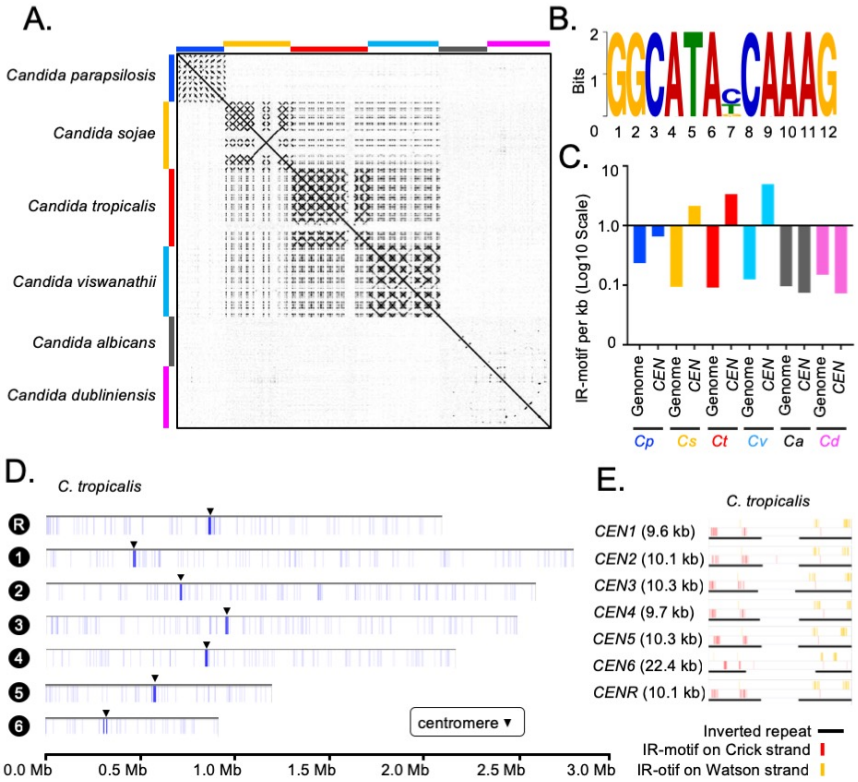
A.
Candida parapsilosis
Candida sojae
Candida tropicalis
Candida viswanathii
Candida albicans
Candida dubliniensis
B.
Bits
2
1
0 1 2 3 4 5 6 7 8 9 10 11 12
C.
IR-motif per kb (Log10 Scale)
10
1.0
0.1
0
Genome
CEN
Cp
Cs
Ct
Cv
Ca
Cd
D.
C. tropicalis
R
1
2
3
4
5
6
centromere
0.0 Mb
0.5 Mb
1.0 Mb
1.5 Mb
2.0 Mb
2.5 Mb
3.0 Mb
E.
C. tropicalis
CEN1 (9.6 kb)
CEN2 (10.1 kb)
CEN3 (10.3 kb)
CEN4 (9.7 kb)
CEN5 (10.3 kb)
CEN6 (22.4 kb)
CENR (10.1 kb)
Inverted repeat
IR-motif on Crick strand
IR-otif on Watson strand

Figure 5

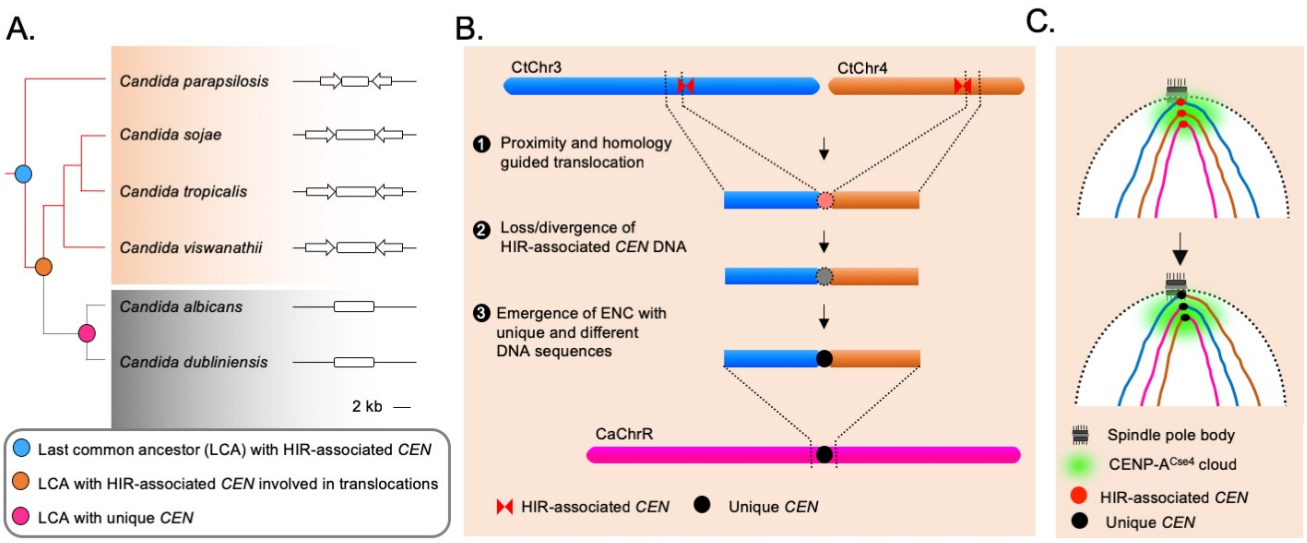
A.
Candida parapsilosis
Candida sojae
Candida tropicalis
Candida viswanathii
Candida albicans
Candida dubliniensis
2 kb
Last common ancestor (LCA) with HIR-associated CEN
LCA with HIR-associated CEN involved in translocations
LCA with unique CEN
B.
CtChr3
CtChr4
1 Proximity and homology guided translocation
2 Loss/divergence of HIR-associated CEN DNA
3 Emergence of ENC with unique and different DNA sequences
CaChrR
HIR-associated CEN
Unique CEN
C.
Spindle pole body
CENP-ACse4 cloud
HIR-associated CEN
Unique CEN